Observation of Spin-Selective Tunneling in SiGe Nanocrystals

G. Katsaros, V. N. Golovach, P. Spathis, N. Ares, M. Stoffel, F. Fournel, O. G. Schmidt, L. I. Glazman, and S. De Franceschi

Phys. Rev. Lett. **107**, 246601 — Published 7 December 2011

DOI: 10.1103/PhysRevLett.107.246601

Observation of spin-selective tunneling in SiGe nanocrystals

G. Katsaros,[1,*] V. N. Golovach,[1] P. Spathis,[1] N. Ares,[1] M. Stoffel,[2]
F. Fournel,[3] O. G. Schmidt,[2] L. I. Glazman,[4] and S. De Franceschi[1]

[1] *SPSMS, CEA-INAC/UJF-Grenoble 1, 17 Rue des Martyrs, 38054 Grenoble Cedex 9, France*
[2] *Institute for Integrative Nanosciences, IFW Dresden, Helmholtzstr. 20, D-01069 Dresden, Germany*
[3] *CEA, LETI, MINATEC, F38054 Grenoble, France*
[4] *Department of Physics, Yale University, New Haven, Connecticut 06520, USA*

Spin-selective tunneling of holes in SiGe nanocrystals contacted by normal-metal leads is reported. The spin selectivity arises from an interplay of the orbital effect of the magnetic field with the strong spin-orbit interaction present in the valence band of the semiconductor. We demonstrate both experimentally and theoretically that spin-selective tunneling in semiconductor nanostructures can be achieved without the use of ferromagnetic contacts. The reported effect, which relies on mixing the light and heavy holes, should be observable in a broad class of quantum-dot systems formed in semiconductors with a degenerate valence band.

The spin-orbit interaction (SOI) has become of central interest in the past years [1], because it enables an all-electrical manipulation of the spin. In the field of spin qubits, one of us [2] suggested the electrical control of localized spins by means of the electric-dipole spin resonance, and this scheme has been successfully used for spin rotations of electrons in quantum dots (QDs) [3, 4]. Already much earlier, Datta and Das [5] proposed a semiconductor transistor that would operate through a gate-controlled spin precession, mediated by the SOI. In this type of spin transistor, spin-polarized electrons are injected into the semiconductor from a ferromagnetic (FM) contact. The realization of an efficient spin injection has proven to be a difficult task [6, 7]. Only recently, high spin-injection efficiencies were reported for FM contacts to semiconductors [8–10]. In nanostructures, however, experimental evidence of spin injection is not as strong and clear [11–15]. Here we show that the SOI in the valence band, quantified by the spin-orbital splitting $\Delta_{\rm SO}$, provides an alternative way to obtain spin-selective tunneling without requiring FM electrodes.

At cryogenic temperatures, transport through QDs is dominated by the Coulomb blockade (CB) effect. In the CB regime, single-hole transport is suppressed and electrical conduction is due to second-order cotunneling (CT) processes [16]. We consider here the case of a QD with an odd number of holes and a spin-doublet ground state. A magnetic field, B, lifts the spin degeneracy by the Zeeman energy $E_Z = g\mu_B B$, where g and μ_B are the hole g-factor and Bohr magneton, respectively. Once the bias voltage across the QD exceeds the Zeeman energy, $|eV| > E_Z$, the inelastic CT processes can flip the QD spin, leaving the QD in the excited spin state; hereinafter e is the elementary charge ($e > 0$). The onset of spin-flip inelastic CT manifests itself as a step in the differential conductance, $G = dI/dV$, at $eV = \pm E_Z$ [17].Our measurements reveal a pronounced asymmetry in the step height of G with respect to the polarity of V. The asymmetry is found to depend on the magnitude and direction of B.

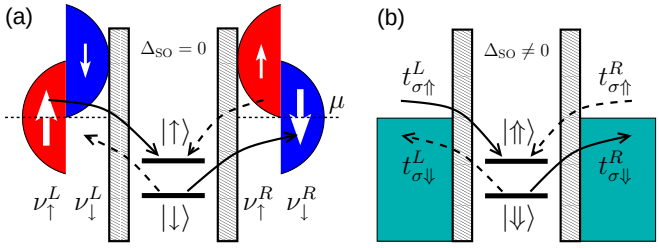

FIG. 1. (color online) Spin-selective tunneling in (a) a QD coupled to FM leads and (b) a QD with SOI coupled to non-magnetic leads. Upon applying a forward (backward) bias, $|eV| \geq E_Z$, the cotunneling processes indicated by the solid (dashed) arrows become allowed. In both (a) and (b), the tunnel rate, $\Gamma \equiv \pi\nu\,|t|^2$, differs for each Zeeman sublevel of the QD. In (a), it is the density of states ν that brings about the spin selectivity of the tunneling. In (b), the spin selectivity is caused by the tunneling amplitude t, which depends on the spinor wave functions at the point of tunneling. In the valence band, the B-field efficiently makes Γ spin-dependent by affecting the mixing between heavy and light holes. Since the inelastic CT current is proportional to $\Gamma^L_\Uparrow\Gamma^R_\Downarrow$ for the forward bias and to $\Gamma^R_\Uparrow\Gamma^L_\Downarrow$ for the reverse bias, an asymmetric $G(V)$ is expected whenever $\Gamma^L_\Uparrow\Gamma^R_\Downarrow \neq \Gamma^R_\Uparrow\Gamma^L_\Downarrow$.

Such kind of asymmetry has been recently predicted by Paaske *et al.*, in a model with a rather generic form of the SOI interaction [18]. In order to understand the observed dependence of the asymmetry on the direction and magnitude of the magnetic field we developed a theory specific for the degenerate valence band of a semiconductor with large Δ_{SO}.

It is interesting to note that the transport characteristics of a QD with SOI coupled to normal leads are similar to those of a QD without SOI coupled to FM leads. We illustrate this similarity in Fig. 1, where we consider the simplest case, in which the Zeeman interaction and the two spin-selective tunnel contacts have collinear quantization directions.

We have studied the low-temperature magneto-transport properties of individual SiGe self-assembled

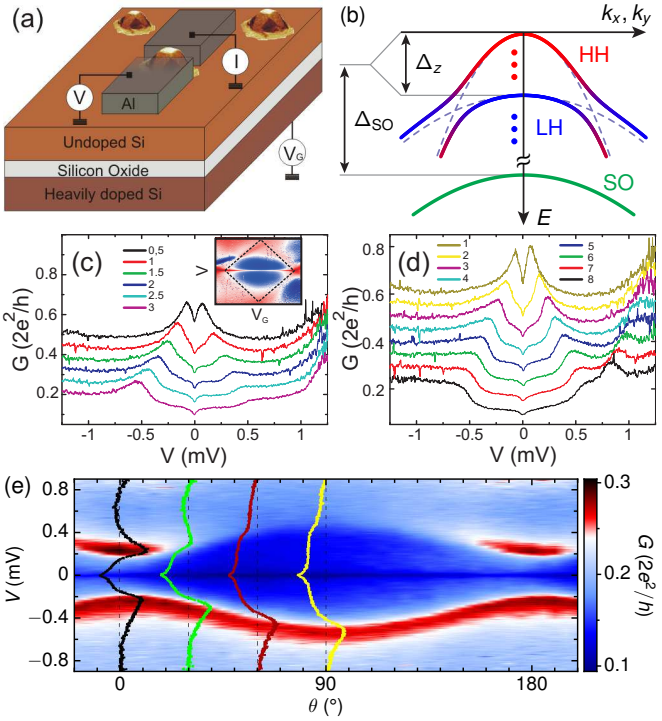

FIG. 2. (color online) (a) Schematic of a QD device fabricated from a SiGe self-assembled nanocrystal grown on a silicon-on-insulator substrate having a heavily doped handle wafer which is used as a back gate [19]. (b) Qualitative band diagram of a Ge-rich SiGe quantum well illustrating the effect of quantum confinement along the growth (z) direction: HH and LH branches are split at $k_x = k_y = 0$ and anti-cross at finite k_x or k_y. In our system, the splitting energy $\Delta_z \sim \gamma_2/mw^2$ is much smaller than the spin-orbital energy Δ_{SO}. The red (blue) dots indicate that many other HH (LH) subbands exist before the first LH (split off) subband is encountered. (c) $G(V)$ for different perpendicular B-fields from 0.5 to 3 T. The traces have been shifted by $0.06 \times 2e^2/h$ for clarity. Inset: $G(V_G, V)$ for a 75-mT perpendicular field needed to suppress the superconductivity of the Al electrodes. (V_G spans a range of 850 mV and V ranges from -3.5 to 3.5 mV). (d) $G(V)$ for different parallel fields from 1 to 8 T. The traces have been shifted by $0.06 \times 2e^2/h$ for clarity. The Zeeman splitting of the Kondo peak is asymmetric in (c) and symmetric in (d). (e) Angular dependence of the split Kondo peak for a fixed V_G and $B = 3$ T. Superimposed $G(V)$ traces for $\theta = 0$, 30, 60, and 90 degrees. The V-shape dip of G at zero bias observed in (c)-(e) is caused by electron-electron interaction in disordered leads [20, 21].

QDs with a base diameter $d \approx 80$ nm and a height $w \approx 20$ nm. A schematic of a typical QD contacted with Al electrodes is shown in Fig. 2(a). For such QDs, the hole wave function is generally composed of both heavy holes (HHs) and light holes (LHs). Due to the confinement and compressive strain, the degeneracy between the HH and LH branches, present in bulk at the Γ-point, is lifted. In Fig. 2(b), we illustrate the interaction between a HH and a LH branch in the two-dimensional (2D) case. The split-

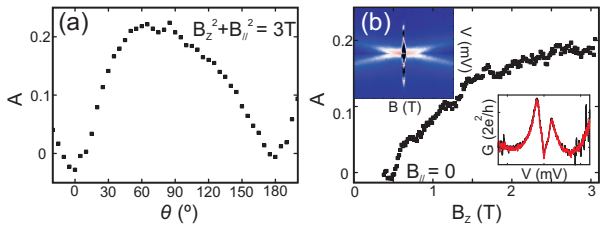

FIG. 3. (color online) Asymmetry parameter A as a function of (a) θ and (b) perpendicular B. We note that, by subtracting the elastic CT contribution from $G(V)$, A becomes larger than 0.5. The top inset in (b) shows the evolution of the Kondo peak while sweeping B_z from -1 to 1 T. The lower insert shows two characteristic line traces taken at -1 T (red) and 1 T (black) demonstrating that $A(B_z) = A(-B_z)$.

off band is far away in energy due to a large Δ_{SO}. HHs and LHs are states of angular momentum $\frac{3}{2}$ with projections $\pm\frac{3}{2}$ and $\pm\frac{1}{2}$, respectively. In the QD, the states consist of a mixture of HH and LH wave functions. In spite of a predominant HH character, symmetry considerations on the constituent Bloch functions imply that, for a realistic device geometry, tunneling to and from the QD states takes place via the LH wave functions. Since LHs cannot be factorized into orbital and spin components, an applied magnetic field induces a spatial variation in the relative orbital "weights" of the two spins. Therefore, the ratio of tunneling amplitudes for "up" and "down" spins will depend on the position of the contacts. In a 2D geometry, this effect should be highly anisotropic since only a perpendicular field has an effect on orbital motion.

The measurements have been performed in a dilution refrigerator with a base temperature of 15 mK. The stability diagram, $G(V_G, V)$, of a QD device is shown in the inset of Fig. 2(c). This device has a charging energy of about $1 - 2$ meV and the orbital level separation is some hundreds of μeV. The diamond-shape region delimited by dashed lines highlights the CB regime for an odd number of confined holes. While G is generally suppressed within this CB diamond, a G resonance can be identified at $V = 0$, providing a clear signature of the Kondo effect [22, 23]. At finite B, this resonance is split by the Zeeman effect as shown in Figs. 2 (c) and (d) for perpendicular and parallel B, respectively.

For perpendicular B [Fig. 2(c)], the splitting of the Kondo peak is clearly asymmetric with respect to a sign change in V. The asymmetry in G arises at the onset of spin-flip inelastic CT (i.e. for $|eV| > E_Z$). For parallel B, however, the asymmetry is practically absent [Fig. 2(d)]. To further investigate this anisotropy, a sequence of $G(V)$ traces was taken while rotating a 3 T field in a plane perpendicular to the substrate. The resulting data, $G(\theta, V)$, are shown in Fig. 2(e), with θ being the angle between $\boldsymbol{B}$ and the substrate plane. Along with a variation in

the Zeeman splitting of the Kondo peak, caused by the θ-dependent hole g-factor [19], the asymmetry becomes progressively more pronounced when going from $\theta = 0$ (or 180°) towards $\theta = 90°$.

The asymmetry observed in $G(V)$ can be quantified by $A = \frac{G_- - G_+}{G_- + G_+}$, where $G_\pm = G(\pm E_Z/e)$. The detailed $A(\theta)$ dependence, extracted from Fig. 2(e), is shown in Fig. 3(a). $A \approx 0$ for $\theta = 0$ (or 180°) and it increases monotonically up to 0.2 for θ approaching 90°; the $A(B)$ dependence is shown in Fig. 3(b). By sweeping the magnetic field from negative to positive values [see insets in Fig. 3 (b)], we further observe that the asymmetry A obeys the relation

$$A(B_z) = A(-B_z). \tag{1}$$

The same qualitative behavior described above was observed in a second device, which did not display Kondo effect, see Supplementary Material. The asymmetry A reaches 0.4 at 3 T for that device. We remark that, although the first device shows larger conductance due to the Kondo effect, the asymmetry A in both devices is a consequence of spin-dependent tunnel rates [25].

In order to understand the microscopic origin of the measured effect, we represent the Luttinger Hamiltonian [24] as a block matrix in the basis of HH (h) and LH (l) states,

$$H = \begin{pmatrix} H_{hh} & H_{hl} \\ H_{lh} & H_{ll} \end{pmatrix}. \tag{2}$$

In H_{hh} and H_{ll}, we discard all terms that vanish in the 2D limit ($w/d \to 0$), whereas in H_{hl} and H_{lh}, we keep only the leading-order terms. A systematic expansion around the 2D limit is outlined in the Supplementary Material. The blocks H_{hh} and H_{ll} assume a familiar form

$$H_{hh/ll} = \frac{\gamma_1 \pm \gamma_2}{2m}\left(k_x^2 + k_y^2\right) + \frac{\gamma_1 \mp 2\gamma_2}{2m}k_z^2 + \frac{1}{2}\mu_B \boldsymbol{\sigma}\cdot g_{h/l}\cdot \boldsymbol{B} + U(x,y) + V_{h/l}(z), \tag{3}$$

where the axes x, y, and z point along the main crystallographic directions, with $z \equiv [001]$ being the direction of the strongest quantization. After the expansion around the 2D limit, the kinetic momentum operators k_x and k_y contain only the component B_z, whereas k_z is independent of $\boldsymbol{B}$. In Eq. (3) and below, γ_1, γ_2, γ_3, κ, and q denote the Luttinger parameters [24] and m denotes the bare electron mass. The Pauli matrices $\boldsymbol{\sigma} = (\sigma_x, \sigma_y, \sigma_z)$ represent the remaining pseudo-spin degree of freedom in each block. We choose the following pseudo-spin basis [26]:

$$\begin{aligned} |\uparrow\rangle_h &= |3/2, -3/2\rangle, \quad |\downarrow\rangle_h = |3/2, +3/2\rangle, \\ |\uparrow\rangle_l &= |3/2, +1/2\rangle, \quad |\downarrow\rangle_l = |3/2, -1/2\rangle. \end{aligned} \tag{4}$$

In the (x, y, z)-frame, the tensors of the g-factor are diagonal: $g_h = \mathrm{diag}\,(0, 0, -6\kappa)$ and $g_l = \mathrm{diag}\,(4\kappa, 4\kappa, 2\kappa)$, where we neglected, for simplicity, the terms proportional to the smallest Luttinger parameter q. The minus sign in $(g_h)_{zz}$ is due to our basis choice in Eq. (4). In Eq. (3), we included an in-plane confining potential $U(x, y)$. The motion along z is confined to an infinitely-deep square well, with different offsets, V_h and $V_l > V_h$, due to strain.

The blocks H_{hl} and H_{lh} are given by

$$H_{hl} = (H_{lh})^\dagger = i\frac{\sqrt{3}\gamma_3}{m}\left(k_x\sigma_y + k_y\sigma_x\right)k_z. \tag{5}$$

These blocks intermix HHs and LHs, such that the wave function of the hole in a given QD state assumes the general form $\Psi = \alpha\Psi_h + \beta\Psi_l$. In terms of the true-spin states, such a wave function consists of a superposition of the spin-up ($\uparrow$) and spin-down ($\downarrow$) states entangled with the orbital degrees of freedom:

$$\begin{aligned} \Psi_\Uparrow(\boldsymbol{r}) &= \Phi_1(\boldsymbol{r})\uparrow + \chi_1(\boldsymbol{r})\downarrow, \\ \Psi_\Downarrow(\boldsymbol{r}) &= \chi_2(\boldsymbol{r})\uparrow + \Phi_2(\boldsymbol{r})\downarrow, \end{aligned} \tag{6}$$

where $\Uparrow$ and $\Downarrow$ denote the components of the Kramers doublet in the QD. Focusing on the first HH subband, we obtain by perturbation theory:

$$\begin{aligned} \Phi_1(\boldsymbol{r}) &= \frac{\sqrt{2}\gamma_3}{m}\mathcal{U}_- k_-\psi_h(x,y)\sum_n f_n^l(z)\frac{\langle f_n^l|\, k_z\,|f_1^h\rangle}{E_1^h - E_n^l}, \\ \chi_1(\boldsymbol{r}) &= \mathcal{U}_-\psi_h(x,y)f_1^h(z) + \frac{2\gamma_3}{m}Zk_-\psi_h(x,y) \\ &\quad\times\sum_n f_n^l(z)\frac{\langle f_n^l|\, k_z\,|f_1^h\rangle}{E_1^h - E_n^l}, \end{aligned} \tag{7}$$

and similar expressions for $\Phi_2(\boldsymbol{r})$ and $\chi_2(\boldsymbol{r})$, obtained from Eq. (7) by replacing $\mathcal{U}_- \to \mathcal{U}_+$, $k_- \to k_+$, and $\psi_h(x,y) \to \psi_h^*(x,y)$. In our notation, $\mathcal{U}_\pm = \mp\frac{1}{\sqrt{2}}(X \pm iY)$ and $k_\pm = \mp\frac{1}{\sqrt{2}}(k_x \pm ik_y)$. The Bloch amplitudes X, Y, and Z describe the valence band in the absence of SOI. In blocks H_{hh} and H_{ll}, the motion along z separates; we denote the corresponding eigenenergies and eigenfunctions by $E_n^{h/l}$ and $f_n^{h/l}(z)$, respectively.

The tunneling amplitudes $t_{\sigma s}^i$ are found as

$$t_{\sigma s}^i = \sum_{u=X,Y,Z} T_u \langle u, \sigma|\Psi_s(\boldsymbol{r}_i)\rangle, \tag{8}$$

where T_u is the coupling strength between Bloch amplitude u and the lead, and $\langle u, \sigma|\Psi_s(\boldsymbol{r}_i)\rangle$ are the projections of the QD eigenstates $\Psi_s(\boldsymbol{r})$, see Eq. (6), onto the product state of Bloch amplitude u and spinor $|\sigma\rangle$. The tunneling amplitudes in Eq. (8) depend on the point of tunneling, $\boldsymbol{r}_i = \boldsymbol{r}_L, \boldsymbol{r}_R$, the component of the true spin in the lead, $\sigma = \uparrow, \downarrow$, and the component of the Kramers doublet on the dot, $s = \Uparrow, \Downarrow$. We remark that T_X, T_Y, and T_Z appear in Eq. (8) as phenomenological parameters. They depend on the details of the metal-semiconductor interface and cannot be determined within the $\boldsymbol{k}\cdot\boldsymbol{p}$-theory used here. We find

$$t_{\sigma s}^i \propto \begin{pmatrix} \bar{\Phi}_1(\boldsymbol{r}_i) & \bar{\chi}_2(\boldsymbol{r}_i) \\ \bar{\chi}_1(\boldsymbol{r}_i) & \bar{\Phi}_2(\boldsymbol{r}_i) \end{pmatrix}, \tag{9}$$

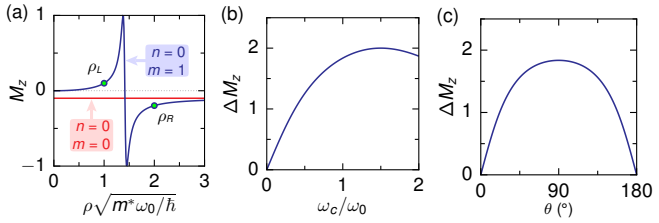

FIG. 4. (color online) (a) Tunneling polarization M_z as a function of the space coordinate ρ for two Fock-Darwin states (n, m) as indicated and for $\omega_c = 0.1\omega_0$. (b) B-field dependence of the difference $\Delta M_z = M_z(\rho_L) - M_z(\rho_R)$, for the values of ρ_L and ρ_R indicated in (a). (c) ΔM_z as a function of θ for a fixed value of $|\boldsymbol{B}|$. The value of $|\boldsymbol{B}|$ corresponds to $\omega_c = \omega_0$ at $\theta = 90°$.

where $\bar{\Phi}_i(\boldsymbol{r})$ and $\bar{\chi}_i(\boldsymbol{r})$ are obtained from Eq. (7) by replacing $Z \to T_Z$ and $\mathcal{U}_\pm \to \mp\frac{1}{\sqrt{2}}(T_X \pm iT_Y)$.

The spin selectivity of the tunneling is best seen in the matrix of the tunnel rates, $\Gamma_{ss'} = \pi \sum_\sigma t^*_{\sigma s}\nu_\sigma t_{\sigma s'}$. With $\nu_\uparrow = \nu_\downarrow$ (case of non-FM leads) we find, up to a common factor,

$$\begin{pmatrix} \Gamma_{\Uparrow\Uparrow} & \Gamma_{\Uparrow\Downarrow} \\ \Gamma_{\Downarrow\Uparrow} & \Gamma_{\Downarrow\Downarrow} \end{pmatrix} \propto \begin{pmatrix} \left|\bar{\Phi}_1\right|^2 + \left|\bar{\chi}_1\right|^2 & \bar{\Phi}^*_1\bar{\chi}_2 + \bar{\chi}^*_1\bar{\Phi}_2 \\ \bar{\Phi}^*_2\bar{\chi}_1 + \bar{\chi}^*_2\bar{\Phi}_1 & \left|\bar{\Phi}_2\right|^2 + \left|\bar{\chi}_2\right|^2 \end{pmatrix}. \tag{10}$$

At $B = 0$, time-reversal symmetry requires that

$$\Phi_2(\boldsymbol{r}) = [\Phi_1(\boldsymbol{r})]^* \quad \text{and} \quad \chi_2(\boldsymbol{r}) = -[\chi_1(\boldsymbol{r})]^*, \tag{11}$$

leading to $\Gamma_{\Uparrow\Uparrow} = \Gamma_{\Downarrow\Downarrow}$ and $\Gamma_{\Uparrow\Downarrow} = \Gamma_{\Downarrow\Uparrow} = 0$ in Eq. (10).

At $B \neq 0$, however, the orbital effect of the B-field modifies the functions $\Phi_i(\boldsymbol{r})$ and $\chi_i(\boldsymbol{r})$, such that the relations in Eq. (11) are no longer satisfied. In general, the matrix $\Gamma_{ss'}$ has nonzero off-diagonal elements. Since it is a hermitian matrix, there exists a direction in space, $\boldsymbol{M}$, such that a rotation of the quantization axis to the direction of $\boldsymbol{M}$ makes the rate matrix diagonal, $\Gamma = \mathrm{diag}(\Gamma_\Uparrow, \Gamma_\Downarrow)$, with $\Gamma_\Uparrow \geq \Gamma_\Downarrow$. To quantify the spin selectivity of the tunneling, we define

$$|\boldsymbol{M}| = \frac{\Gamma_\Uparrow - \Gamma_\Downarrow}{\Gamma_\Uparrow + \Gamma_\Downarrow}. \tag{12}$$

In respect to transport, $\boldsymbol{M}$ is analogous to the polarization vector of the FM lead. Indeed, the maximum of spin selectivity in tunneling from a FM is achieved when the FM is a half-metal, *e.g.*, $\nu_\uparrow \neq 0$ and $\nu_\downarrow = 0$. This extreme case corresponds to $M = 1$ and can be approached in our case by increasing B_z.

In order to illustrate the origin of the spin selectivity, we focus on the special case: $T_X = T_Y = 0$ and $T_Z \neq 0$ and refer to this tunneling model as the Z-model. In the Z-model, $\boldsymbol{M}$ is parallel to the z-axis. Tunneling to the hole states is possible only due to the admixture of the LH subbands. Furthermore, in this model, the spin selectivity is determined by the fact that $\bar{\chi}_1(\boldsymbol{r}) \propto k_-\psi_h(x, y)$ and $\bar{\chi}_2(\boldsymbol{r}) \propto k_+\psi^*_h(x, y)$, whereas $\bar{\Phi}_i(\boldsymbol{r}) \equiv 0$. Using this information in Eqs. (10) and (12), we specify $\psi_h(x, y)$ to the Fock-Darwin states [27]. Therefore, we assume that $U(x, y)$ in Eq. (3) is given by $U(\rho) = m^*\omega_0^2\rho^2/2$, where m^* is the effective mass for in-plane motion, ω_0 is the oscillator frequency of the harmonic potential, and $\rho^2 = x^2 + y^2$. For the first two states ($n = 0$ and $m = 0, -1$), we obtain

$$M_z = -\frac{\omega\omega_c}{\omega^2 + \omega_c^2/4}, \tag{13}$$

where $\omega = \sqrt{\omega_0^2 + \omega_c^2/4}$, and $\omega_c = eB_z/m^*c$. For these states, M_z depends on B_z but not on ρ, see Fig. 4(a). For $B_z \neq 0$, the contacts will exhibit spin-dependent tunnel rates with the same polarization value M_z regardless of position of the tunneling point. In such a case, no asymmetry in the inelastic CT is expected.

For higher energy levels, M_z may depend on ρ,

$$M_z = \left[\frac{\omega}{\omega_c}f(\rho) + \frac{\omega_c}{4\omega}\frac{1}{f(\rho)}\right]^{-1}, \tag{14}$$

where $f(\rho)$ is given for arbitrary n and m in Supplementary Material. We consider further the state $n = 0$ and $m = 1$, for which $f(\rho) = 2\hbar/(m^*\omega\rho^2) - 1$. Now M_z depends both on B_z and on ρ, see Fig. 4(a). The spin polarization of two contacts positioned arbitrarily on a QD may differ significantly from each other, see, *e.g.*, points ρ_L and ρ_R in Fig. 4(a). The asymmetry in the inelastic CT is related to $\Delta M_z = M_z(\rho_L) - M_z(\rho_R) \neq 0$. ΔM_z increases with B_z [Fig. 4 (b)], displaying at the same time strong dependence on the B-field direction [Fig. 4 (c)], in good qualitative agreement with the results in Fig. 3.

Finally, our theory also explains the symmetry relation in Eq. (1). On the one hand, the spin-selective part of $\Gamma_{ss'}$ is proportional to B_z and therefore it changes sign when flipping the direction of the magnetic field. On the other hand, the Zeeman energy also changes sign when flipping the direction of the magnetic field, exchanging thus the roles of the ground and the excited state. Therefore, A does not change upon $\boldsymbol{B} \to -\boldsymbol{B}$.

The described joint effect of SOI and Zeeman splitting explains our experimental findings. In addition, it opens the door to an original scheme for measuring Rabi spin oscillations in QDs confining holes. Let us consider a spin-1/2 QD in the CB regime under a perpendicular B of the order of a few T. In such a case, a transport characteristic of the type shown in Fig. 2(c) is to be expected. For $V = 0$, no current flows through the QD. Yet we suggest that a finite current could be generated by a resonant rf field (at frequency $f = E_Z/h$) capable of inducing coherent oscillations between the Zeeman-split states of the QD. In fact, as the excited $\Uparrow$ state becomes populated it can decay to the ground $\Downarrow$ state by an inelastic CT process—a hole tunnels out of the QD from the $\Uparrow$ state being replaced by another hole tunneling into the $\Downarrow$ state. Because $\Uparrow$ and $\Downarrow$ states have tunnel couplings

with opposite asymmetries, in a configuration such as the one depicted in Fig. 1(b) the most favorable CT relaxation process would involve the transfer of a hole from the right to the left contact. Hence a net dc current could be driven by a continuous resonant irradiation. In addition, combining rf bursts with synchronized V_G pulses may enable the coherent control of the QD pseudo-spin states. In this scheme, well-defined pseudo-spin rotations would be performed in the deep CB regime (i.e. during a negative V_G pulse), whereas pseudo-spin read-out would take place in the CT regime.

We acknowledge J. Paaske for helpful discussions and A. Rastelli and H. von Kaenel for providing the STM image used in Fig. 2(a). The work was supported by the Agence Nationale de la Recherche (through the ACCESS and COHESION projects), US DOE Contract No. DE-FG02-08ER46482 (Yale), and the Nanosciences Foundation at Grenoble, France. G.K. acknowledges support from the Deutsche Forschungsgemeinschaft.

* Present address: Institute for Integrative Nanosciences, IFW Dresden, Helmholtzstr. 20, D-01069 Dresden, Germany, email: g.katsaros@ifw-dresden.de

[1] R. Winkler, *Spin-Obit Coupling Effects in Two-Dimensional Electron and Hole Systems* (Springer 2003).
[2] V. N. Golovach *et al.*, Phys. Rev. B **74**, 165319 (2006).
[3] K. C. Nowack *et al.*, Science **318**, 1430, (2007).
[4] S. Nadj-Perge *et al.*, Nature **468**, 1084 (2010).
[5] S. Datta, and B. Das, Appl. Phys. Lett. **56**, 665 (1990).
[6] I. Žutić *et al.*, Rev. Mod. Phys. **76**, 323 (2004).
[7] E.I. Rashba, Semicond. Sci. Technol. **23**, 114015 (2008).
[8] H. C. Koo *et al.*, Science **325**, 1515 (2009).
[9] I. Appelbaum *et al.*, Nature **447**, 295 (2007).
[10] C.H. Li *et al.*, *Nature Communications*, DOI: 10.1038/ncomms1256, (2011).
[11] K. Tsukagoshi *et al.*, Nature **401**, 572 (1999).
[12] S. Sahoo *et al.*, Nat. Phys. **1**, 99 (2005).
[13] K. Hamaya *et al.*, Phys. Rev. B **77**, 081302(R) (2008).
[14] F.A. Zwanenburg *et al.*, Nano Lett. **9**, 2704 (2009).
[15] E.-S. Liu *et al.*, Nano Lett. **10**, 3297 (2010).
[16] S. De Franceschi *et al.*, Phys. Rev. Lett. **86**, 878 (2001).
[17] A. Kogan *et al.*, Phys. Rev. Lett. **93**, 166602 (2004).
[18] J. Paaske *et al.*, Phys. Rev. B **82**, 081309(R) (2010).
[19] G. Katsaros *et al.*, Nature Nanotechnology **5**, 458, (2010).
[20] B. L. Altshuler and A. G. Aronov, *Electron-Electron Interactions in Disordered Systems* (Elsevier, Amsterdam, 1985).
[21] F. Pierre *et al.*, Phys. Rev. Lett. **86**, 1589 (2001).
[22] D. Goldhaber-Gordon *et al.*, Nature **391**, 156-159 (1998).
[23] O. Klochan *et al.*, Phys. Rev. Lett. **107**, 076805 (2011).
[24] See Eq. (45) in J.M. Luttinger, Phys. Rev. **102**, 1030 (1956).
[25] To exclude experimental artifacts, we verified that A changes sign upon exchanging the source and drain leads.
[26] The advantage of this choice is that the pseudo-spin transforms under the time reversal as a spin 1/2, i.e. $|\uparrow\rangle \rightarrow |\downarrow\rangle$ and $|\downarrow\rangle \rightarrow -|\uparrow\rangle$.
[27] V. Fock, Z. Phys. **47**, 446 (1928); C.G. Darwin, Proc. Cambridge Philos. Soc. **27**, 86 (1930).